the upper critical field, H_{c2}. The square FLL, shown in the top row of Fig. 3, is stable below 2 kOe for all temperatures. We note that although the magnetic order below T_N is also square symmetric, other effects, including in-plane Fermi surface anisotropy[16] and H_{c2} anisotropy[17], can stabilize the square FLL. As the square FLL is stable in most of the superconducting phase outside the regime of magnetic ordering, this symmetry certainly cannot be solely attributed to the magnetic order. In the magnetically ordered state, coincident with the transition at 2 kOe, the FLL undergoes a rhombic distortion, as shown in the middle of row of Fig. 3. The two rhombohedral domains, rotated by 90°, are each distorted by 15° ± 1°, the same angular splitting as seen in the new magnetic modulation in this region. This symmetry remains stable between 3 and 4 kOe. Above 4 kOe, the FLL undergoes a second transition into two hexagonal domains, also rotated by 90°, shown in the bottom row of Fig. 3. This cannot be an extension of the low-field rhombohedral distortion, as that would result in hexagonal domains orientated in the [100] direction, rather than the observed [110] as is evident from Fig. 3. Instead, this change in orientation implies a discontinuous transition. Above 4 kOe, all 12 magnetic reflections are of equal intensity, giving the same number of reflections as the FLL, albeit with a symmetry distorted from pure hexagonal. The origin of the FLL symmetry transitions in relation to magnetic transition is still an open question, as we cannot from the present data determine if one drives the other or *vice versa*.

It is important to point out the difference between the symmetry transitions reported here, and our previous reports of the low-field transition ($H < 1$ kOe) in $ErNi_2B_2C$ (ref. 10), and YNi_2B_2C and $LuNi_2B_2C$ (ref. 11) where the transitions proceed continuously through a rhombic distortion and is understood from anisotropic flux line interactions due to the high in-plane anisotropy of the Fermi surface[16]. The low-field region was not probed in the SANS measurements, but Bitter decorations at 50 Oe and 4.2 K verified a hexagonal FLL. Previous studies of the interaction between magnetism and the superconducting FLL in $ErNi_2B_2C$ showed a rotation due to the internal field direction and a disordering due to increased pinning[9]. We believe that these effects, while convincing evidence of the strong coupling between the two types of order, can be understood within the scattering time approximation. The observations reported in here will require a deeper and more subtle understanding.

The splitting of the magnetic peaks with wavevector $\mathbf{q}_{mII}$ can be suppressed between 4 and 10 kOe by cooling the sample in the saturated paramagnetic state and then reducing the field into the hexagonal FLL state. Such low-temperature hysteresis is common in magnetic systems. In $HoNi_2B_2C$, hysteresis in the metamagnetic transitions has been reported[18], and in $DyNi_2B_2C$ the associated residual moment has been seen to suppress superconductivity[19]. This hysteresis is not seen in the FLL. If the FLL is the determining factor in this problem, then this hysteresis in the split of the magnetic modulation could be ascribed to passing through a FLL symmetry transition. Further studies into the details of the symmetries and the transitions between them are needed to identify the driving mechanisms, and to shed more light on the intimate connection between superconductivity and magnetism in this material. □

Received 31 December 1997; accepted 23 March 1998.

1. Crabtree, G. W. *et al.* Anisotropic superconducting and magnetic properties of a single crystal of $ErRh_4B_4$. *Phys. Rev. Lett.* **49,** 1342–1345 (1982).
2. Siegrist, T. *et al.* The crystal structure of superconducting $LuNi_2B_2C$ and the related phase LuNiBC. *Nature* **367,** 254–256 (1994).
3. Cava, R. J. *et al.* Superconductivity in the quaternary intermetallic compounds $LnNi_2B_2C$. *Nature* **367,** 252–253 (1994).
4. Nagarajan, R. *et al.* Bulk superconductivity at an elevated temperature ($T_c \approx 12$ K) in a nickel containing alloy system Y-Ni-B-C. *Phys. Rev. Lett.* **72,** 274–277 (1994).
5. Cho, B. K. *et al.* Magnetic and superconducting properties of single-crystal $TmNi_2B_2C$. *Phys. Rev. B* **52,** 3676–3683 (1995).
6. Lynn, J. W. *et al.* Magnetic order and crystal structure in the superconducting $RNiB_2C_2$ materials. *Phys. Rev. B* **55,** 6584–6598 (1997).
7. Sternlieb, B. *et al.* Single crystal diffraction study of the magnetic structure of $TmNi_2B_2C$. *J. Appl. Phys.* **81,** 4937–4939 (1997).
8. Cho, B. K. *et al.* Magnetism and superconductivity in single crystal $ErNi_2B_2C$. *Phys. Rev. B* **52,** 3684–3695 (1995).
9. Yaron, U. *et al.* Microscopic coexistence of magnetism and superconductivity in $ErNi_2B_2C$. *Nature* **382,** 236–238 (1996).
10. Eskildsen, M. R. *et al.* Observation of a field-driven structural phase transition in the flux line lattice in $ErNi_2B_2C$. *Phys. Rev. Lett.* **78,** 1968–1971 (1997).
11. Eskildsen, M. R. *et al.* Structural stability of the square flux line lattice in YNi_2B_2C and $LuNi_2B_2C$ studied with small angle neutron scattering. *Phys. Rev. Lett.* **79,** 487–490 (1997).
12. Gammel, P. L. *et al.* Small angle neutron scattering study of the magnetic flux-line lattice in single crystal 2*H*-$NbSe_2$. *Phys. Rev. Lett.* **72,** 278–282 (1994).
13. Kleiman, R. N. *et al.* Neutron diffraction from the vortex lattice in the heavy-fermion superconductor UPt_3. *Phys. Rev. Lett.* **69,** 3120–3124 (1992).
14. Gray, K. E. Ginzburg-Landau equations, interphase surface energy, and the intermediate state of superconductors with a paramagnetic normal state. *Phys. Rev. B* **27,** 4157–4160 (1983).
15. Tachiki, M., Matsumoto, H. & Umezawa, H. Mixed state in magnetic superconductors. *Phys. Rev. B* **20,** 1915–1927 (1979).
16. Kogan, V. G. *et al.* Vortex lattice transitions in borocarbides. *Phys. Rev. B* **55,** R8693–R8696 (1997).
17. De Wilde, Y. *et al.* Scanning tunneling microscopy observation of a square Abrikosov lattice in $LuNi_2B_2C$. *Phys. Rev. Lett.* **78,** 4273–4277 (1997).
18. Canfield, P. C. Angular dependence of metamagnetic transitions in $HoNi_2B_2C$. *Phys. Rev. B* **55,** 970–976 (1997).
19. Peng, Z. Q., Krug, K. & Winzer, K. Large hysteresis effect and reentrant behavior in $DyNi_2B_2C$ at temperatures $T < 2$ K. *Phys. Rev. Lett.* (submitted).

Acknowledgements. We thank C. Stassis, P. Hedegård and J. Jensen for discussions. This work was supported by NATO. M.R.E. is supported by the Danish Research Academy, D.G.N. is supported by the Robert A. Welch Foundation and P.C.C. is supported by the Director of Energy Research, Office of Basic Energy Science.

Correspondence and requests for materials should be addressed to M.R.E. (e-mail: morten.eskildsen@risoe.dk).

Simulated response of the ocean carbon cycle to anthropogenic climate warming

Jorge L. Sarmiento*, Tertia M. C. Hughes*, Ronald J. Stouffer† & Syukuro Manabe†‡

** Program in Atmospheric and Oceanic Sciences, Princeton University, PO Box CN710, Princeton, New Jersey 08544, USA*
† Geophysical Fluid Dynamics Laboratory/NOAA Princeton University, PO Box 308, Princeton, New Jersey 08542, USA

A 1995 report[1] of the Intergovernmental Panel on Climate Change provides a set of illustrative anthropogenic CO_2 emission models leading to stabilization of atmospheric CO_2 concentrations ranging from 350 to 1,000 p.p.m. (refs 1–4). Ocean carbon-cycle models used in calculating these scenarios assume that oceanic circulation and biology remain unchanged through time. Here we examine the importance of this assumption by using a coupled atmosphere–ocean model of global warming[5] for the period 1765 to 2065. We find a large potential modification to the ocean carbon sink in a vast region of the Southern Ocean where increased rainfall leads to surface freshening and increased stratification[6]. The increased stratification reduces the downward flux of carbon and the loss of heat to the atmosphere, both of which decrease the oceanic uptake of anthropogenic CO_2 relative to a constant-climate control scenario. Changes in the formation, transport and cycling of biological material may counteract the reduced uptake, but the response of the biological community to the climate change is difficult to predict on present understanding. Our simulation suggests that such physical and biological changes might already be occurring, and that they could substantially affect the ocean carbon sink over the next few decades.

We use the GFDL atmosphere–ocean climate model[7] to which we

‡ Present address: Earth Frontier Research System, 7th Floor, Seavans Building-N, 1-2-1 Shibaura, Minato-ku, Tokyo 105, Japan.

have coupled an ocean carbon model[8]. A constant climate 'control' model fixes CO_2 and other long-lived greenhouse gases at their initial value. The global warming ('GW') model is that of Haywood *et al.*[5], which includes estimates of the radiative forcing based on observed CO_2 (Fig. 1a) and other long-lived greenhouse gases from 1765 to 1990, and predicted future increases of these gases until 2065 (see Methods). Also included is an estimate of the direct effect of sulphate aerosols. The model prediction of warming in global mean surface air temperatures is in reasonable agreement with observations[5]. Despite limitations in the model, and our inability to know whether the climate sensitivity of this model is correct, the fact that the model reproduces the observed temperature record encourages us to use it as a framework for examining the response of the global carbon cycle to climate change in the next century.

The ocean carbon component of the coupled atmosphere–ocean model solves the full carbon system equations and includes the 'biological pump' (in which organic matter and $CaCO_3$ are formed at the ocean surface, then sink and are released at depth) parametrized as in the previous century-scale coupled model study[8] of Sarmiento and Le Quéré (Fig. 1b; see Methods). Given our present understanding, any model of how biology will respond to global warming must be considered highly speculative. Our approach was to run a simple model based on assuming a minimum change in the production and export of organic matter and $CaCO_3$. This 'constant-biota' model fixes the production and export at their initial values except where the major nutrient phosphate becomes depleted at the surface, in which case production is set to zero. Such a fixed production model might be expected if whatever limits growth in the present ocean (for example, iron supply by windborne dust[9]) were to remain constant. We fix the time history of atmospheric CO_2 as in Fig. 1a and allow the CO_2 to invade the ocean. One simulation was performed in the control climate model to provide a 'baseline' with constant climate. This is similar to the assumption of constant ocean circulation (except that climate variability is included) that was made in the Intergovernmental Panel on Climate Change (IPCC) CO_2 stabilization models[1–4]. A second simulation was performed in the GW model.

We find that the constant-biota GW model takes up almost as much CO_2 as the constant-biota baseline model (Fig. 1b; rows A and E of Table 1). The 1980–89 mean annual uptake is in the middle of the IPCC estimate of 2.0 ± 0.8 Pg C yr^{-1} for ocean models without global warming[1]. However, an analysis of the processes contributing to the global warming simulation reveals that, without the biological pump, there would be a very large negative influence on the oceanic uptake owing to warming of the ocean and changes in transport (Fig. 1c; rows B and C of Table 1). The solubility GW model that we use to isolate these processes (see Methods) shows a divergence from its baseline beginning before ~1970 (Fig. 1c). By 1990 the cumulative solubility GW uptake is 27 Pg C lower than its baseline, and by 2065 the decrease is 124 Pg C (rows B and C of Table 1). The latter is about half of the total fossil CO_2 emissions from the beginning of the industrial revolution until today. The constant-biota model counteracts these decreases, but we need to know whether other scenarios would do the same.

As a reasonable lower limit to the impact of the biological pump, we examined a 'constant phosphate' model that fixes the surface phosphate content through time, such as might be expected if the primary limit to phytoplankton growth were a limiting micronutrient that is supplied primarily from within the ocean (for example, possibly dissolved iron supplied by deep waters of the present Southern Ocean[10]). The 1990 to 2065 cumulative uptake in the constant phosphate model (Fig. 1b) is 219 Pg C. This is 79 Pg C less than its control run, as contrasted with a difference of only 27 Pg C for the constant-biota model. An upper-limit model of complete phosphate consumption (a 'super-biotic' model similar to the iron-fertilization scenario explored by Sarmiento and Orr[11] and to one of the proposed hypotheses for the lowering of CO_2 during the last ice age[12–14]) shows a 1990 to 2065 cumulative uptake of 409 Pg C. Although such an extreme scenario would never be realized, it is clear, from the range between the lower limit of 219 Pg C and the super-biotic uptake of 409 Pg C, that changes in biology could easily modify the ocean carbon sink substantially between now and the middle of the twenty-first century.

An important result of the simulations is that most of the impact

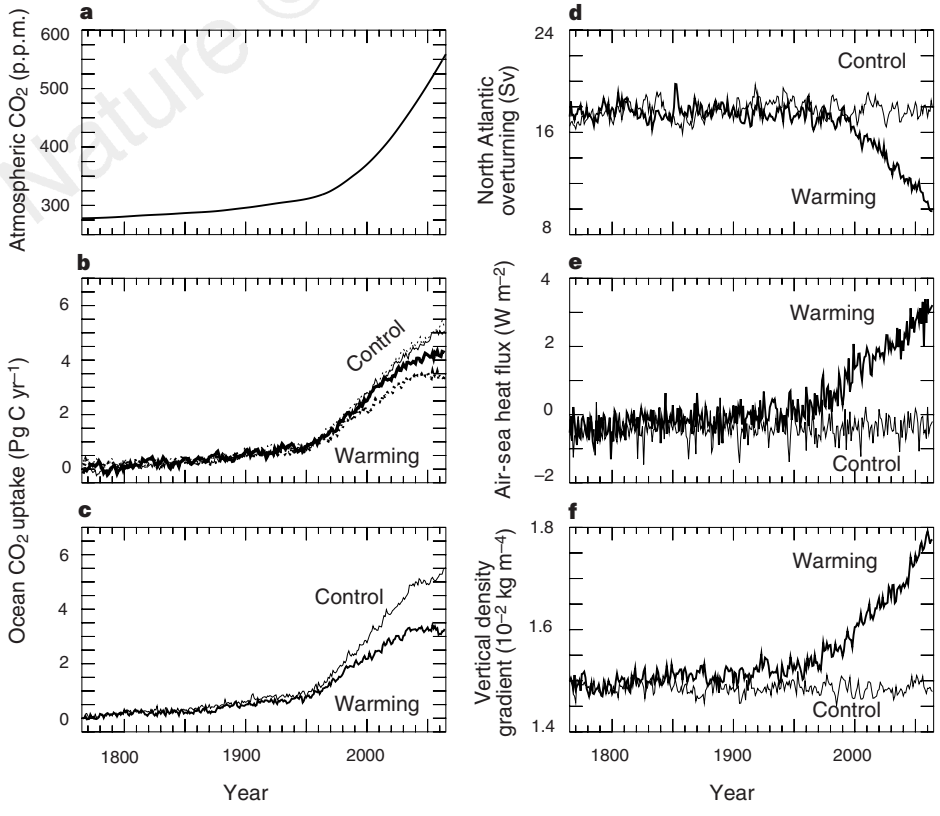

Figure 1 Time series of model boundary conditions and predictions. **a**, Atmospheric CO_2 based on observations before 1990 and the IPCC IS92a model[23] thereafter. **b**, Annual ocean uptake of carbon by the biology model. Four simulations are shown: the constant-biota control model (thin solid line), the constant-biota GW model (thick solid line), the constant-phosphate control model (thin dotted line) and the constant-phosphate GW model (thick dotted line). **c**, Annual ocean uptake of carbon by the 'solubility' model. **d**, Maximum value of overturning in the thermohaline cell of the North Atlantic in units of Sverdrups ($1\ Sv = 10^6\ m^3\ s^{-1}$). **e**, Global mean of the air–sea heat flux. **f**, Global mean vertical density gradient at the base of the first layer of the model (50.9 m) for latitudes polewards of 30° in both hemispheres.

Table 1 Oceanic uptake of anthropogenic CO_2 in constant-biota model

	Annual uptake (Pg C yr^{-1})		Cumulative uptake (Pg C)	
	1980–89	2056–65	1765–1990	1990–2065
A. Constant-biota baseline	1.96	5.03	112	289
B. Change due to variation in transport processes in absence of biological pump*	–0.17	–1.54	–5	–63
C. Change due to warming in absence of biological pump†	–0.20	–0.50	–23	–33
D. Change due to biological pump‡	+0.40	+1.26	+39	+69
E. Global warming constant-biota model	1.99	4.25	123	262

* The change due to variation in transport processes is calculated from the difference between the solubility baseline model and a solubility 'constant-temperature' GW scenario in which surface temperature was kept constant for calculation of surface carbon chemistry. An analysis of the transport out of the surface layer shows that the processes that decrease are vertical mixing and convective overturning. In contrast, advective transport increases. During the final decade of the simulation, the ratio of the decrease in convection to mixing is 0.24:0.76. The change in vertical mixing is mostly (>90%) accounted for by the isopycnic component, which is decreased owing to the change in the slope of the isopycnals. The advective contribution increases by an amount equal to 38% of the decrease in convective transport.
† The change due to warming is calculated by taking the difference between the solubility GW and solubility constant-temperature GW simulations.
‡ The biological contribution is estimated by taking the difference between the global warming constant-biota result and the constant biota baseline plus the change due to warming and the change in ocean transport processes in the solubility model; that is, D = E − (A + B + C).

of warming and transport processes (as well as the compensatory effect of biology) occurs in the Southern Ocean (Fig 2a and b). A primary reason for the importance of the Southern Ocean is its dominance in the global oceanic uptake of anthropogenic carbon[15]. Similar changes that occur in the high latitudes of the North Atlantic are larger by unit area but smaller in total impact owing to the relatively small total area that is involved.

Because of the importance of the high latitudes in the carbon cycle response to global warming, it is tempting to ascribe the observed effects to changes in deep-water formation, as was suggested for an idealized century-scale study with the same model as ours[8]. In support of this, our simulations show a marked decrease in the circulation of North Atlantic Deep Water beginning as early as the next decade (Fig. 1d). However, in the period between now and the middle of the twenty-first century, this and other changes in vertical advection have very little impact on the oceanic uptake of carbon from the atmosphere. Indeed, the region of the Southern Ocean where the maximum changes in air–sea flux occur is characterized by massive upwelling due to Ekman divergence. This upwelling actually increases slightly in response to the global climate warming.

An analysis of the term balances in the upper layer of the model shows that the decrease in uptake in the solubility GW model is due primarily to the net flux of heat into the ocean (perturbation heat flux) that results from climate warming (which decreases CO_2 solubility) (Table 1; Fig. 1e and 2c), and a decrease in the magnitude of the vertical component of isopycnic mixing and convective overturning (Table 1; Fig. 2d). Note that the correct diagnostic for the effect of heating on the air–sea CO_2 flux is the perturbation of the atmosphere–ocean heat flux, which measures the present rate at which the ocean is being heated. The increase in temperature that results from this input of heat (which is concentrated at lower latitudes than the perturbation of the heat flux) is a diagnostic for the integrated effect of heating, not of its instantaneous rate. The heat flux perturbation effect predominates in the early period, accounting for 82% of the decrease in the cumulative uptake from 1765 to 1990 (Table 1). However, between 1990 and 2065, transport processes (mixing, convective overturning and advection) account for 66% of the decrease in cumulative uptake; during the final decade, the contribution of transport processes has increased to 75% of the decrease.

The high-latitude heat flux perturbation and changes in ocean transport processes are a consequence of increased stratification of the upper water column (Fig. 1f). The increased stratification causes

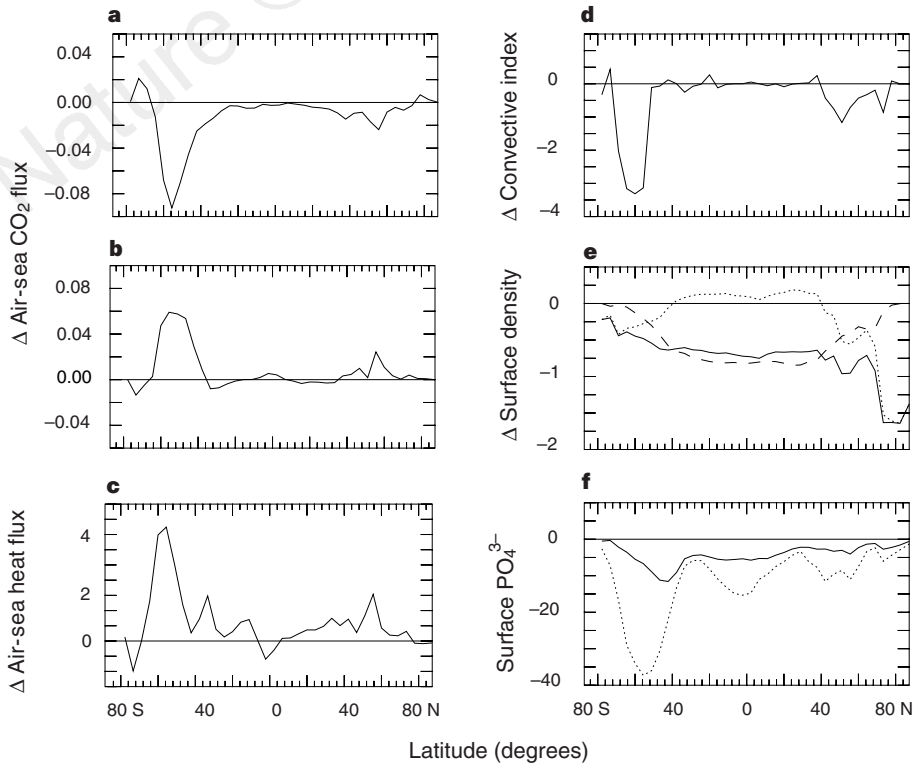

Figure 2 Zonal integrals for the decade 2056–65 of: **a**, the change in air–sea CO_2 fluxes (positive for ocean uptake) due to warming and changes in ocean transport estimated by the difference between the solubility GW and the solubility baseline (Pg degree^{-1} yr^{-1}); **b**, the change in air–sea CO_2 fluxes due to the biological pump estimated by taking the difference between the constant-biota GW and the constant-biota baseline air–sea CO_2 fluxes, after removing the changes due to warming and transport (Pg degree^{-1} yr^{-1}); **c**, GW minus baseline heat fluxes in W m^{-1}; and **d**, GW minus baseline of the convection index (10^5 m times the fraction of the year during which convection occurs at the base of the first model layer). **e**, Zonal mean change in surface density (GW minus control model in units of kg m^{-3}). The solid line is the total change in density. The dashed and dotted lines are the density changes due to temperature and salinity, respectively. **f**, Zonal integral (solid line) for the decade 2056–65 of constant biota GW minus constant biota baseline surface phosphate concentration in mmol m^{-2}. Also shown (dotted line) is the negative of the surface phosphate concentration in the baseline scenario. Note that the phosphate depletion is substantially less than the phosphate available in almost all latitude bands.

the decrease in vertical mixing along isopycnals (which are now more horizontal) as well as the decrease in convective overturning (Fig. 2d). These changes in transport decrease the vertical transport of carbon. They also decrease the upward mixing of warm waters from below. Because of this, surface temperatures do not increase as much as elsewhere, and even cool in some regions[16], with the consequence that the perturbation of the heat flux is greatest in the Southern Ocean. The increased stratification also causes a gradual collapse of the thermohaline circulation[6] in the entire deep ocean, which has a major role in the carbon balance on century timescales[8].

Increased stratification at the surface is a global phenomenon resulting from increased temperature in low latitudes and freshening in high latitudes (Fig. 2e). In this connection we note that an earlier ocean-only study of the carbon cycle response to global warming over the industrial period was forced with warming but did not include changes in hydrology[17]. In our coupled model, the freshening of the high latitudes by increased precipitation is crucial to determining the response of the ocean carbon cycle to global warming[6]. The anthropogenic carbon uptake predicted by the previous study and our constant biota model are similar over the next 50–60 years, but the mechanisms driving that response are different.

The enhancement of atmospheric CO_2 uptake by the biological pump in the constant-biota simulation also occurs primarily in the high latitudes of the Southern Ocean (Fig. 2b), mirroring the decrease in CO_2 uptake in the solubility GW model (Fig. 2a). The dominance of the Southern Ocean is again due to its sensitivity to the changes in stratification and to the fact that this is the region of the world in which deep mixing is normally able to reach into the vast volume of deep water that holds excess biogenic carbon[11]. The effect of the biological model on the air–sea flux of CO_2 depends on how the biological pump responds to the increased stratification and changes in ocean transport. We initialize the biological model with the downward biological pump flux in balance with the upward transport of excess dissolved inorganic carbon and nutrients; that is, there is no initial net flux of CO_2 across the air–sea interface. The slowing of vertical exchange in the GW model breaks this balance by decreasing the upward supply of excess dissolved inorganic carbon. The continued downward flux of organic carbon and $CaCO_3$ in the constant-biota GW model leads to an accumulation of excess biogenic dissolved inorganic carbon in the deep ocean. A diagnostic of the effect of decreased upward supply of deep carbon and nutrients in the constant-biota simulation is the decrease in surface phosphate concentration (Fig. 2f). The phosphate that is removed from the surface is accompanied by carbon. The resulting decrease in surface dissolved inorganic carbon leads to an increase in anthropogenic CO_2 uptake. The constant-phosphate model has a much smaller effect on the surface dissolved inorganic carbon concentration because it does not decrease the surface phosphate concentration.

An important caveat regarding our results is that all the ocean transport processes that change are parametrizations of phenomena that are not resolved by the model. It is urgent that simulations such as ours be attempted with models with different parametrizations of mixing and convection[18]. If similar results are obtained, we would urge consideration of a major international effort to monitor the Southern Ocean for changes in temperature, salinity and vertical stratification, as well as changes in the biological pump; and to study the processes that determine the response of the Southern Ocean to global warming. Our understanding of biological processes, in particular, is still rudimentary[19].

Detection of changes in the carbon balance due to the biological pump should be possible, although challenging. Atmospheric oxygen is a possible tracer. Between 1995 and 2065, we infer an increase of 283 p.p.m. in the ratio of atmospheric oxygen to nitrogen in the constant-biota model. This signal (equivalent to 59 p.p.m. CO_2, with the addition of a carbon atom[20]) would be readily detectable[20,21], but would have to be isolated from the signals from fossil fuel burning and terrestrial biota[20]. The contribution of oceanic warming to the oxygen signal could possibly be isolated from other processes by using changes in the atmospheric concentration ratio of noble gases to nitrogen (which differ in the temperature sensitivity of their solubilities; R. Keeling, personal communication). Another possible tracer of change is oceanic oxygen, whose global mean decreases by $-8\,\mathrm{mmol\,m^{-3}}$ between 1990 and 2065. Locally, at a depth of ~1,600 m in the Southern Ocean, large regions southeast of the Pacific and south of the Indian Ocean show a decrease of more than $-20\,\mathrm{mmol\,m^{-3}}$, with troughs in excess of $-50\,\mathrm{mmol\,m^{-3}}$. These changes would be easy to measure, but present models are not sufficiently reliable to indicate where those regions would be. □

Methods

The GW climate model includes radiative forcing from CO_2 plus the effect of other long-lived greenhouse gases represented as their equivalent in CO_2. The estimated direct effect of sulphate aerosols is represented as an increase in surface reflectance. The thermal forcing is similar to that of Mitchell *et al.*[22], with an increase of ~1% per year after 1990, which is similar to the IPCC IS92a model[23]. The GW model does not include changes in radiative forcing by ozone or soot, changes in solar forcing, or the indirect effect of aerosols. The atmosphere and ocean models have approximately 4° horizontal resolution.

The biological pump consists of: (1) the formation of organic matter and $CaCO_3$ at the surface of the ocean; (2) export to depth by sinking of particulate organic matter and $CaCO_3$, as well as transport of dissolved organic matter; and (3) metabolization of organic matter and dissolution of $CaCO_3$ in the deep ocean to form 'excess' dissolved inorganic carbon and nutrients. The initial magnitude of the biological pump is determined before coupling the ocean model to the atmospheric model by requiring that the model fit the observed surface distribution of phosphate[8,24]. The ratio of organic carbon to phosphorus is fixed at 120:1, with half the production going into particulate organic matter and half into dissolved organic carbon. Particulate organic matter is metabolized following a scaling depth obtained from sediment trap observations[25]. Dissolved organic matter is metabolized as a first-order decay process. The ratio of $CaCO_3$ to phosphorus production and dissolution is determined at each depth level of the model by forcing the horizontal mean alkalinity profile predicted by the model towards observations. The $CaCO_3$-to-phosphorus ratio is fixed after coupling the ocean model to the atmosphere model. We ignore the small sediment burial term of both organic matter and $CaCO_3$.

Before coupling the ocean carbon model to the atmosphere–ocean climate model, we determine the total carbon content by fixing atmospheric CO_2 at 277.95 μatm and allowing it to invade the ocean-only model until the air–sea flux goes to zero. After the ocean carbon model has been coupled to the climate model, the coupled model is run for an additional 250 years with a fixed atmospheric CO_2 concentration before beginning the global warming simulations. The model is then run from 1765 to 2065 with atmospheric CO_2 increasing as in Fig. 1a and invading the ocean by gas exchange with a windspeed-dependent gas-exchange coefficient[26]. In our predictions of anthropogenic CO_2 uptake, we ignore sediment dissolution of $CaCO_3$ and changes in calcification rates that would buffer the oceanic carbon chemistry. An important aspect of future increases in atmospheric CO_2 is that they will occur too rapidly for the sediment dissolution buffering mechanism to have a role until much later[27].

The solubility model is identical to the biological simulation except that the biological pump is removed. An additional change is to decrease the total amount of alkalinity in the ocean to the salinity-normalized mean of surface observations ($2{,}379\,\mathrm{meq\,m^{-3}}$ at a salinity of 35‰, as contrasted with the global mean of $2{,}477\,\mathrm{meq\,m^{-3}}$ at a salinity of 35‰ used in the biological model). This is done so that the surface carbon buffer capacity in the solubility model is comparable to that in the biological model. The solubility model permits us to examine the effect of warming and changes in ocean circulation without the biological response.

Received 7 November 1997; accepted 13 March 1998.

1. Schimel, D. *et al.* in *Climate Change 1995* (ed. Houghton, J. T.) 76–86 (Cambridge Univ. Press, 1996).
2. Schimel, D. *et al.* in *Climate Change 1994* (ed. Houghton, J. T.) 35–71 (Cambridge Univ. Press, 1995).

3. Enting, I. G., Wigley, T. M. L. & Heimann, M. *Future Emissions and Concentrations of Carbon Dioxide: Key Ocean/atmosphere/land Analyses* (CSIRO Division of Atmospheric Research, 31, 1994).
4. Sarmiento, J. L., Le Quéré, C. & Pacala, S. W. Limiting future atmospheric carbon dioxide. *Glob. Biogeochem. Cycles* **9,** 121–138 (1995).
5. Haywood, J. M., Stouffer, R. J., Wetherald, R. T., Manabe, S. & Ramaswamy, V. Transient response of a coupled model to estimate changes in greenhouse gas and sulfate concentrations. *Geophys. Res. Lett.* **24,** 1335–1338 (1997).
6. Manabe, S. & Stouffer, R. J. Century-scale effects of increased atmospheric CO_2 on the ocean–atmosphere system. *Nature* **364,** 215–218 (1993).
7. Manabe, S., Stouffer, R. J., Spelman, M. J. & Bryan, K. Transient responses of a coupled ocean–atmosphere model to gradual changes of atmospheric CO_2. Part 1: annual mean response. *J. Clim.* 785–818 (1991).
8. Sarmiento, J. L. & Le Quéré, C. Oceanic carbon dioxide uptake in a model of century-scale global warming. *Science* **274,** 1346–1350 (1996).
9. Coale, K. H. *et al.* A massive phytoplankton bloom induced by an ecosystem-scale iron fertilization experiment in the equatorial Pacific Ocean. *Nature* **383,** 495–501 (1996).
10. Johnson, K. S., Gordon, R. M. & Coale, K. H. What controls dissolved iron concentrations in the world ocean? *Mar. Chem.* **57,** 137–161 (1997).
11. Sarmiento, J. L. & Orr, J. C. Three-dimensional simulations of the impact of Southern Ocean nutrient depletion on atmospheric CO_2 and ocean chemistry. *Limnol. Oceanogr.* **36,** 1928–1950 (1991).
12. Siegenthaler, U. & Wenk, T. Rapid atmospheric CO_2 variations and ocean circulation. *Nature* **308,** 624–626 (1984).
13. Sarmiento, J. L. & Toggweiler, J. R. A new model for the role of the oceans in determining atmospheric pCO_2. *Nature* **308,** 621–624 (1984).
14. Knox, F. & McElroy, M. Changes in atmospheric CO_2, influence of marine biota at high latitudes. *J. Geophys. Res.* **89,** 4629–4637 (1984).
15. Sarmiento, J. L., Orr, J. C. & Siegenthaler, U. A perturbation simulation of CO_2 uptake in an ocean general circulation model. *J. Geophys. Res.* **97,** 3621–3646 (1992).
16. Manabe, S. & Stouffer, R. J. Multiple century response of a coupled ocean–atmosphere model to an increase of atmospheric carbon dioxide. *J. Clim.* **7,** 5–23 (1994).
17. Maier-Reimer, E., Mikolajewicz, U. & Winguth, A. Future ocean uptake of CO_2: interaction between ocean circulation and biology. *Clim. Dyn.* **12,** 711–721 (1996).
18. Gent, P. R., Willebrand, J., McDougall, T. J. & McWilliams, J. C. Parameterizing eddy-induced tracer transports in ocean circulation models. *J. Phys. Oceanogr.* **25,** 463–474 (1995).
19. Denman, K., Hofmann, E. & Marchant, H. in *Climate Change 1995* (ed. Houghton, J. T.) 483–516 (Cambridge Univ. Press, 1996).
20. Keeling, R. F., Najjar, R. P., Bender, M. L. & Tans, P. P. What atmospheric oxygen measurements can tell us about the global carbon cycle. *Glob. Biogeochem. Cycles* **7,** 37–68 (1993).
21. Bender, M., Ellis, T., Tans, P., Francey, R. & Lowe, D. Variability in the O_2/N_2 ratio of southern hemisphere air, 1991–1994: implications for the carbon cycle. *Glob. Biogeochem. Cycles* **10,** 9–22 (1996).
22. Mitchell, J. F. B., Johns, T. C., Gregory, J. M. & Tett, S. F. B. Climate response to increasing levels of greenhouse gases and sulphate aerosols. *Nature* **376,** 501–504 (1995).
23. Houghton, J. T., Callander, B. A. & Varney, S. K. (eds) *Climate Change 1992* (Cambridge Univ. Press, 1992).
24. Sarmiento, J. L., Murnane, R. & Quéré, C. L. Air–sea CO_2 transfer and the carbon budget budget of the North Atlantic. *Phil. Trans. R. Soc. Lond. B* **348,** 211–218 (1995).
25. Martin, J. H., Knauer, G. A., Karl, D. M. & Broenkow, W. W. VERTEX: carbon cycling in the northeast Pacific. *Deep-Sea Res.* **34,** 267–285 (1987).
26. Wanninkhof, R. Relationship between wind speed and gas exchange over the ocean. *J. Geophys. Res.* **97,** 7373–7383 (1992).
27. Archer, D., Kheshgi, H. & Maier-Reimer, E. Multiple timescales for the neutralization of fossil fuel CO_2. *Geophys. Res. Lett.* **24,** 405–408 (1997).

Acknowledgements. We thank Corinne Le Quéré for adding the carbon component ot the coupled model, Fortunat Joos for providing the atmospheric CO_2 figures, and Jerry Mahlman and Yasuhiro Yamanaka, as well as Klaus Keller, Francois Morel, Phillippe Tortell and Ernst Maier-Reimer, for comments. The contributions of J.L.S. and T.M.C.H. were supported by the Office of Global Programs of the National Oceanic and Atmospheric Administration, and by the National Science Foundation. The paper was written in part while J.L.S. was visiting the Bermuda Biological Station for Research with support from EXXON Corporation; J.L.S. thanks Tony Knap for making the arrangements.

Correspondence and requests for materials should be addressed to J.L.S. (e-mail: jls@splash.princeton.edu).

Dynamic responses of terrestrial ecosystem carbon cycling to global climate change

Mingkui Cao* & F. Ian Woodward

Department of Animal and Plant Sciences, University of Sheffield, Sheffield SI0 2TN, UK

Terrestrial ecosystems and the climate system are closely coupled, particularly by cycling of carbon between vegetation, soils and the atmosphere. It has been suggested[1,2] that changes in climate and in atmospheric carbon dioxide concentrations have modified the carbon cycle so as to render terrestrial ecosystems as substantial carbon sinks[3,4]; but direct evidence for this is very limited[5,6]. Changes in ecosystem carbon stocks caused by shifts between stable climate states have been evaluated[7,8], but the dynamic responses of ecosystem carbon fluxes to transient climate changes are still poorly understood. Here we use a terrestrial biogeochemical model[9], forced by simulations of transient climate change with a general circulation model[10], to quantify the dynamic variations in ecosystem carbon fluxes induced by transient changes in atmospheric CO_2 and climate from 1861 to 2070. We predict that these changes increase global net ecosystem production significantly, but that this response will decline as the CO_2 fertilization effect becomes saturated and is diminished by changes in climatic factors. Thus terrestrial ecosystem carbon fluxes both respond to and strongly influence the atmospheric CO_2 increase and climate change.

Ecosystem carbon fluxes are controlled by the processes of photosynthesis, plant (autotrophic) respiration and soil (heterotrophic) respiration. The difference between plant photosynthesis and respiration is defined as net primary production (NPP), and the difference between NPP and soil respiration, defined as net ecosystem production (NEP), represents the net carbon flux from the atmosphere to ecosystems. Among many factors affecting these processes, the most obvious at the global scale are elevated CO_2 concentration and climate change, which directly and indirectly influence and interact to control the carbon fluxes from ecological and physiological processes[1,2]. We have used the carbon exchange between vegetation, soil and the atmosphere (CEVSA) model[9] to assess the dynamic responses of natural terrestrial ecosystems to CO_2 increases and climate change from the onset of industrialization (the 1860s) to a doubling of current radiative forcing, which will be reached in the 2060s based on IPCC scenario IS92a (ref. 11). The model simulates the processes of stomatal conductance, evapotranspiration, plant photosynthesis and respiration, nitrogen uptake, carbon allocation among plant organs, litter production, nitrogen mineralization and soil organic carbon decomposition, and uses these to calculate the carbon fluxes between vegetation, soils and the atmosphere. We do not include the effects of nitrogen deposition and modifications to ecosystem structure and distribution by natural and anthropogenic processes.

The scenarios of transient CO_2 concentration and climate change between 1861 and 2070 used in this study were produced by the Hadley Centre for Climate Prediction and Research, UK Meteorological Office with a coupled ocean–atmospheric general circulation model (GCM), which accounts for the effects of both greenhouse gases and aerosols[10,12]. The concentrations of greenhouse gases and aerosols used by the GCM for the period 1861–1990 were derived from observed data, whereas those after 1990 were based on IPCC scenario IS92a with an increase in CO_2 by 1% yr^{-1} (ref. 11). This climate projection has been appropriately tested against observed trends and spatial patterns of climate[10,12].

We use the CEVSA model and the GCM scenarios of CO_2 and climate change to make simulations at a spatial resolution of 2.5° latitude × 3.75° longitude and a time step of one month. The model is first run with the GCM simulation of pre-industrial climate until an ecological equilibrium is reached, that is when the differences between annual NPP, litter production and soil respiration, and the interannual variations in soil moisture and carbon stocks were less than 0.1%. After reaching this equilibrium, the model is driven by the GCM simulation of the transient changes in CO_2 and climate from 1861 to 2070.

We isolated and combined the effects of elevated CO_2 and climate change by simulations with CO_2 increase but no climate change, climate change but no CO_2 increase, and both CO_2 increase and climate change. In addition to a global-scale analysis, the results are integrated into three latitudinal zones, northern (>40° N), temperate (40° N–20° N and >30° S) and tropical (20° N–30° S)

* Present address: Department of Environmental Sciences, University of Virginia, Charlottesville, Virginia 22903, USA.